Nanoassemblies Designed from Semiconductor Quantum Dots and Molecular Arrays

E. Zenkevich,[‡] F. Cichos,[†] A. Shulga,[‡] E. P. Petrov,[†,§] T. Blaudeck,[†] and C. von Borczyskowski*,[†]

Institute of Physics, Chemnitz University of Technology, 09107 Chemnitz, Germany and National Academy of Sciences, Institute of Molecular and Atomic Physics, Minsk 220072, Belarus

Received: August 31, 2004; In Final Form: November 17, 2004

The formation of nanoassemblies of CdSe/ZnS quantum dots (QD) and pyridyl-substituted free-base porphyrin (H_2P) molecules has been spectroscopically identified by static and time-resolved techniques. The formation of nanoassemblies has been engineered by controlling the type and geometry of the H_2P molecules. Pyridyl functionalization gives rise to a strong complex formation accompanied by QD photoluminescence (PL) quenching. For some of the systems, this quenching is partly related to fluorescence resonance energy transfer (FRET) from the QD to H_2P and can be explained according to the Förster model. The quantitative interpretation of PL quenching due to complexation reveals that (i) on average only about $^1/_5$ of the H_2P molecules at a given H_2P/QD molar ratio are assembled on the QD and (ii) only a limited number of "vacancies" accessible for H_2P attachment exist on the QD surface.

1. Introduction

"Bottom-up" approaches for functionalized nanoassemblies are an intriguing field for both fundamental science and envisaged applications. During the last two decades, considerable progress has been reported in two fields not initially related, that is, nanostructured semiconductor materials prepared by lithographic methods or conventional organometalic synthesis[1−4] and chemical approaches based on supramolecular chemistry.[5−9] In recent years, the merging of both fields has been, besides others, driven by the concept of molecular electronics.[10,11] Following these general trends, considerable progress has been made in the preparation and characterization of both colloidal semiconductor nanocrystals, such as CdSe,[12] and self-assembled molecular architectures.[13,14] Both kinds of nanoassemblies are realized in solution or at solid/liquid interfaces. Only a few attempts to interlink semiconductor nanocrystals and organic chromophores have been reported on a microscopic level.[15−19] Nanocrystals are subject to quantum size effects, and such quantum dots (QD) are often strongly emissive.[4,12] In assemblies of this type, for example, the phenomenon of photosensitized electron injection from organic subunits to semiconductor nanoparticles is used to activate charge separation even at optical excitations below the semiconductor band gap energy.[15−17] In addition, nonradiative energy transfer depending on absorption/emission properties and intercenter distances between interacting nanoparticle-dye moieties strongly influences the dynamics and relaxation pathways in such complex systems.[18,19]

The other driving force for the growing interest in nanoassemblies is, besides fundamental investigations, the use of QD as photoluminescence markers linked to biologically relevant molecules[19−22] and the creation of new optical and laser materials.[23,24] According to these attractive applications, the anchoring of organic molecules to wide band gap semiconductor colloidal nanocrystals is of considerable scientific and practical interest.

The envisaged perspectives of such a combination are broad. Among other reasons, the tunability of the optical band gap of nanocrystals via size-dependent quantum confinement[4,12,16] (optical tunability) and the nearly unlimited possibilities of the chemical engineering of electronic properties of organic molecules (chemical tunability)[5−7,13,14] are, with respect to new material properties, stimulating and promising arguments in concentrating on the architecture of organic−inorganic nanoassemblies.

During the past decade, we have developed a concept to self assemble biomimetic porphyrin arrays that are tunable with respect to photoinduced energy and/or charge transfer. The so-called "key-hole" organization principle is based on the complexation of metal ions in the center of porphyrin macrocycles via suitable ligands such as pyridiyl rings[7,25,26]. We have shown extensively that the complexation is based essentially on a "Lego-type" key-hole principle effectively controllable via steric factors such as distance matching, optimization of relative orientations, and solvent composition.

Recently, we have reported the first successful attempts to extend such concepts to semiconductor colloids and have anchored pyridyl-substituted tetrapyrrolic organic molecules on CdSe/ZnS core/shell semiconductor nanoparticles.[27,28] In addition, it has been reported[16] that the interaction of CdSe/ZnS core/shell nanocrystals with specially designed diazaperylene molecules (having two anchoring nitrogens) manifests itself in a complete quenching of the nanocrystal emission accompanied by the appearance of a new, not yet identified electronic state.

In this publication, we will report in detail for the first time on the extension of the above-outlined self-assembly principle with the final goal being to organize molecular arrays on semiconductor quantum dot surfaces in a systematic way. We intend to make use of both the tunability of the QD band gap via size variation and the chemical engineering of functionalized organic molecules. Although the main emphasis of this paper

* Corresponding author. E-mail: borczyskowski@physik.tu-chemnitz.de
† Chemnitz University of Technology.
‡ National Academy of Sciences.
§ Present address: Institute of Biophysics/BioTec, Dresden University of Technology, 01307 Dresden, Germany.

10.1021/jp040595a CCC: $30.25
Published on Web 04/09/2005

SCHEME 1: Chemical Structure, Abbreviations, and Positions of Mesosubstituents for Porphyrin (H_2P) Molecules

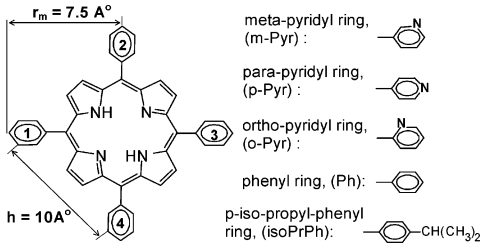

Porphyrin abbreviation	Meso-substituents		λ (nm)/ε(10^3 $M^{-1}\cdot cm^{-1}$)[a]
(m-Pyr)$_1$H$_2$P	1: (m-Pyr)	2, 3, 4: (Ph)	515 / 20.0
(m-Pyr)$_2$H$_2$P	1, 3: (m-Pyr), opposite	2, 4: (Ph)	515 / 19.9
iso(m-Pyr)$_2$H$_2$P	1, 3: (m-Pyr), opposite	2, 4: (iso-PrPh)	515 / 19.9
(m^Pyr)$_2$H$_2$P	1, 2: (m-Pyr), adjacent	3,4: (Ph)	515 / 20.3
iso(m^Pyr)$_2$H$_2$P	1, 2: (m-Pyr), adjacent	3, 4: (iso-PrPh)	516 / 20.3
(m-Pyr)$_3$H$_2$P	1, 2, 3: (m-Pyr)	4: (Ph)	515 / 19.7
(p^Pyr)$_2$H$_2$P	1, 2: (p-Pyr), adjacent	3, 4: (Ph)	514 / 19.5
(m-Pyr)$_4$H$_2$P	1, 2, 3, 4: (m-Pyr)	--	516 / 19.3
(p-Pyr)$_2$H$_2$P	1, 2, 3, 4: (p-Pyr)	--	513 / 19.6
(o-Pyr)$_2$H$_2$P	1, 2, 3, 4: (o-Pyr)	--	513 / 17.5

[a] Wavelengths (λ) of absorption maxima and molar decimal extinction coefficients (ϵ) were measured in toluene. An average total error of the extinction values is 10%.

is on the realization and identification of quantum dot-dye nanoassemblies, we will also describe the energy transfer observed in these systems. In the future, we will aim at controllable dynamics such as photoinduced charge and excitation energy transfer between the individual entities of the nanoassemblies.

2. Materials and Methods

Trioctylphosphine oxide (TOPO)-capped highly monodisperse CdSe nanocrystals were prepared using a modification of the conventional organometallic synthesis.[29] In addition, surface passivation with an inorganic ZnS shell leads to an improvement of the room-temperature quantum efficiency of the photoluminescence (PL) of CdSe up to 40−60%.[30] Two types of CdSe/ZnS nanocrystals were used to form semiconductor nanoparticle-porphyrin composites in toluene (Aldrich spectroscopic grade without further purification) at ambient temperature: "yellow" quantum dots (YQD) ($n = 2$ ZnS monolayers) with the first excitonic maximum in absorption at $\lambda_{max} = 512$ nm and "red" quantum dots (RQD) ($n = 3$) with the first maximum at 556 nm. YQD and RQD have been provided by A. Rogach (Ludwig-Maximilians-University Munich, Germany) and D. Talapin (Hamburg University, Germany). Very similar results have been obtained with the corresponding QD provided by Evident Co, USA.

Because of the well-known phenomenon of quantum confinement of Wannier-Mott excitons in CdSe below its Bohr radius[4,12] ($a_B \sim 50$ Å), colloidal semiconductor CdSe nanocrystals show size-dependent and tunable absorption and PL properties.[4,12,22] Correspondingly, sizes of the QD under study have been estimated from the absorption spectra as recently described[31] on the basis of well-proven experimental dependencies between the position of the first excitonic maximum in absorption and the QD diameter.[32−34] The CdSe diameters amount to $d = 2.5$ nm for YQD and $d = 3.2$ nm for RQD. The size-dependent molar decimal extinction coefficients (ϵ) for the first excitonic maximum in absorption have been determined for these QD using well-established size-to-optical-property relations[16,33−35] and result in the following: $\epsilon(\lambda) = 0.7 \times 10^5$ M^{-1} cm^{-1} at $\lambda_{max} = 512$ nm for YQD and $\epsilon(\lambda) = 1.25 \times 10^5$ M^{-1} cm^{-1} at $\lambda_{max} = 556$ nm for RQD (toluene, 295 K).

We have shown earlier[7,25,26] that selectively replacing phenyl rings in tetraphenyl porphyrins with pyridyl rings opens the possibility of a controllable formation of multiporphyrin assemblies with Zn-porphyrin dimers via a key-hole principle. It is well documented that Zn^{2+} ions having vacant d^{10} orbitals, whereas the heteroatom N (in the pyridyl ring) has a lone pair orbital, form Zn···N−Pyr coordination bonds easily. Experiments have been carried out using mesopyridyl-substituted porphyrins following this scheme of self-aggregated complexation for CdSe/ZnS. Scheme 1 shows the structures and nomenclature of porphyrin free-bases (H_2P) schematically with various numbers (from 1 to 4) of mesopyridyl rings differing by their relative positions with respect to the porphyrin macrocycle (opposite (-) or adjacent (∧)) and to the position (ortho-, meta-, para-) of the nitrogen within the pyridyl ring. In addition, porphyrins with isopropyl-phenyl side chains were used to modify steric interactions with TOPO molecules as well as

improve H_2P solubility. The Table in Scheme 1 contains the absorption maxima (λ) and the corresponding molar decimal extinction coefficients (ϵ) experimentally determined in this work. All of the pyridyl-substituted porphyrin free-bases were synthesized and purified following the reported procedures.[36]

The experimental procedure for the formation of QD-H_2P nanoassemblies was the same as that reported recently.[26] The initial concentration of QD in toluene solutions (in a 10 × 10 mm^2 quartz cuvette) was in the range of C_{QD} (1/2)·10^{-7} M. Porphyrins were added sequentially in steps of 10 μL from a highly concentrated stock solution (C_{porph}(~8×10^{-6})/(4×10^{-5} M)) up to the wanted molar ratios $x = [H_2P]/[QD]$.

A spectrophotometer (Shimadzu UV-3101PC) was used for absorption measurements, whereas a Shimadzu RF-5001PC spectrofluorimeter was used for fluorescence measurements. Prior to performing steady-state fluorescence experiments, the spectrofluorimeter was calibrated for the spectral response of the detection channel against a set of fluorescence standards according to the procedure described recently.[37]

Time-resolved fluorescence measurements were performed in the time-correlated single photon counting (TCSPC) mode under right-angle geometry. A cavity-dumped Rhodamine 6G dye laser (Spectra-Physics models 375B and 344S) pumped synchronously by a mode-locked argon−ion laser (Spectra-Physics model 171) was used to provide a tunable pulsed excitation of about 80 ps fwhm in the range of 570−630 nm. The laser beam was attenuated by neutral density filters to about 50 nJ per pulse at the sample. Because the longest decay components of CdSe/ZnS QD were in the range of 100 ns,[38,39] the repetition frequency of the cavity dumper (Spectra-Physics model 344S) was set to 817 kHz. The photoluminescence was selected spectrally using a monochromator (PTR Optics model SMC-02-22) at a resolution of 3.5 nm. A Peltier-cooled R3809U microchannel plate photomultiplier tube (MCP−PMT Hamamatsu) was used as the fluorescence detector.

Luminescence kinetics were analyzed using an approach based on the recovery of decay time distributions with a minimum of a-priori assumptions on the luminescence decay.[38,40,] Following this procedure, the "true" luminescence decay originates from an (unknown) distribution of decay times $f(\tau)$. In this case, the decay time distribution analysis reduces to the inversion of the quasi-Laplace transform. Details of the decay analysis have been described earlier.[40]

3. Results

3.1. Optical Properties of QD and H_2P. Because pyridine might be more strongly coordinated on CdSe/ZnS QD surfaces[41] than TOPO, we have used pyridyl-substituted porphyrins to attempt similar organization features, as already reported[7,25,26] for both QD and porphyrins. According to the possibilities of the lone pair N orbitals of pyridyls to form coordination bonds with suitable ligating partners such as Zn^{2+} ions, we varied the porphyrin molecule systematically with respect to the pyridyl rings. The respective porphyrin-QD organization principles are, as shown in Scheme 1, the following: (i) the number of pyridyl rings, (ii) the position (ortho-, meta-, para-) of nitrogen atom (N) within the pyridyl ring, and (iii) the relative orientation (opposite, adjacent) of the pyridyl rings with respect to each other.

Figure 1 collects the photoluminescence (PL) and absorption spectra of a 1.7×10^{-7} M solution of YQD (Figure 1, top) and RQD (Figure 1, bottom) as a function of added (*m*-Pyr)$_3$H$_2$P at well-defined molar ratios (x). The absorption spectra in Figure 1 show that upon titration (while increasing x), besides the

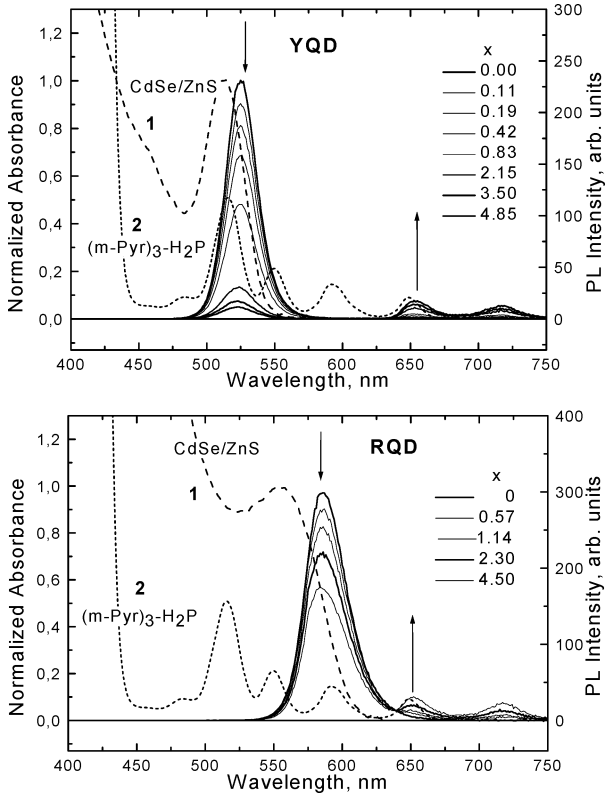

Figure 1. Dependence of CdSe/ZnS QD PL spectra on the molar ratio (x) of (*m*-Pyr)$_3$H$_2$P in toluene at 295 K for YQD at $\lambda_{ex} = 465$ nm (top) and for RQD at $\lambda_{ex} = 575$ nm (bottom). Arrows show the decrease (↓) of CdSe/ZnS QD PL relative intensity (at $\lambda_{max} = 524$ nm for YQD and 585 nm for RQD) and increase (↑) of H_2P fluorescence bands upon increasing x. Curves 1 and 2 correspond to the normalized absorption spectra of CdSe/ZnS QD and (*m*-Pyr)$_3$H$_2$P, respectively.

absorption of QD at 512 (YQD) and 556 nm (RQD), a linear increase of the well-known H_2P absorption bands takes place. The corresponding H_2P fluorescence spectra increase nearly linearly (Figure 1) but show a small (~2 nm) red shift and a change in the Franck−Condon envelope of the overall spectrum. Typical H_2P fluorescence spectra are shown in Figure 2 as a function of x. We would like to note here that the observed spectral shift might be correlated with the quenching efficiency reported later on. Despite the fact that the QD absorption remains constant, the PL at $\lambda_{max} = 512$ nm for YQD and 556 nm for RQD is considerably quenched upon titration with (*m*-Pyr)$_3$H$_2$P. No such effects are observed when using various porphyrins without pyridyl rings.

To gain more insight into the quenching effects, we have investigated the time-resolved PL of RQD. Experiments were limited to RQD because of the available excitation wavelength of our laser system. As can be seen from Figure 3A, the PL of RQD shows, as reported in various other experiments for similar compounds,[38,42] a nonexponential decay. The multiexponential decay has been analyzed as described earlier in the experimental part. The obtained distribution of decay times is shown in Figure 3B. The decay time distribution shows a strong and broad peak centered at 19−22 ns that is related to the "intrinsic" PL of CdSe QD. The large width of the peak reflects that there is, as expected, a remaining size distribution of QD that will result in a distribution of decay times.[38,42] As was reported recently,[43] the center and width of this intrinsic decay component depends noticeably on the excitation and detection wavelength and/or the corresponding bandwidths. It is also seen in Figure 3B that at least two additional time components are observed at ~7 ns

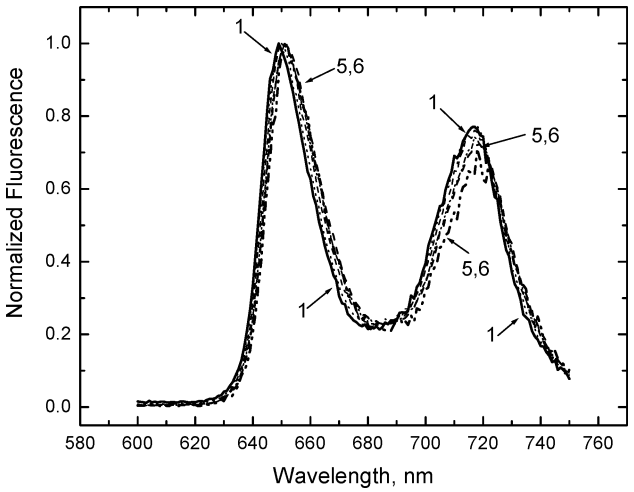

Figure 2. ($m\wedge$Pyr)$_2$H$_2$P fluorescence spectra (normalized to the maximum) in the presence of YQD as a function of the molar ratio (x) (λ_{exc} = 420 nm): 1 (x = 0.55, λ_{max} = 649 nm); 2 (x = 1.09, λ_{max} = 650 nm); 3 (x = 2.16, λ_{max} = 650 nm); 4 (x = 4.25, λ_{max} = 651 nm); 5 (x =8.30, λ_{max} = 651 nm); 6 (pure ($m\wedge$Pyr)$_2$H$_2$P without YQD, λ_{max} = 651 nm).

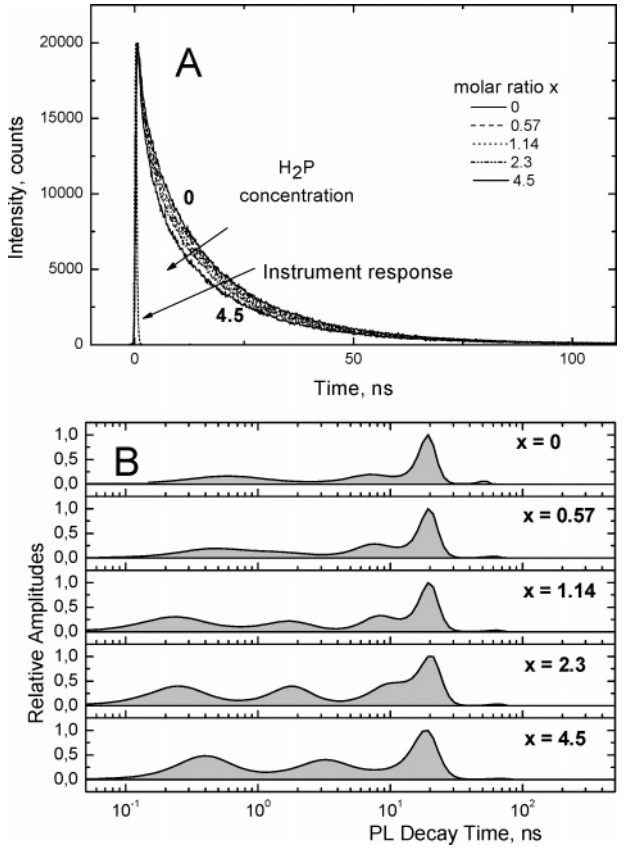

Figure 3. Time-resolved PL traces (A) and decay amplitude distributions (B) for RQD upon increase of the molar ratio (x) of (m-Pyr)$_3$H$_2$P (λ_{exc} = 575 nm, λ_{em} = 585 nm).

and ~700 ps. These components reflect that there is a (static or dynamic) inhomogeneous distribution of RQD, some of them showing (unidentified) nonradiative relaxation processes shortening the intrinsic PL decay. Similar effects have already been reported.[19] The part of RQD that is already subject to quenching processes before adding H_2P amounts to about 25−50% (see also the quantum efficiency (φ_D) given in Table 1). Also, a dynamic disorder of RQD might be responsible for such a time distribution.

The experimental data reveal that the nonexponential behavior increases upon increasing the H_2P molar ratio (x), as is also shown in Figure 3A. The fit results for the PL decay depicted in Figure 3B clearly show (besides the PL lifetime distribution already found for RQD in the absence of H_2P) additional decay components coming up with increasing x. Qualitatively, at least one additional component shows up at about 1−3 ns and is steadily increasing with increasing x. Accompanied with the build-up of this additional component, the remaining decay time distribution changes.

In Figure 4, we show the fluorescence decay analysis of (m-Pyr)$_3$H$_2$P at a detection wavelength of 650 nm (porphyrin Q (0, 0) fluorescence band) in a solution containing only H_2P (Figure 4B) and in the presence of RQD (Figure 4C) at x = 4.5. A strong decay component is observed in both experiments at about 9 ns, as is well known for H_2P in nondegassed liquid solutions at ambient temperature.[7,26] In the presence of RQD (decay time distribution shown in Figure 4C), we observe, as compared to Figure 4B, at least two additional components, namely, a small component at about 20 ns, which is clearly related to the still persisting PL of RQD (see Figure 4A) at the detection wavelength of 650 nm and a small build-up component (with negative amplitude) centered at about 2−3 ns, which indicates a population mechanism of H_2P due to the presence of RQD. At the moment, the nature of this build-up component remains unknown. Additionally, comparing the H_2P component in Figure 4B and C reveals that the corresponding width in the presence of QD is broader by about 25% as compared to pure H_2P. This indicates that the fluorescence lifetime for H_2P molecules is slightly changed and shifted to longer times upon complexation with QD.

3.2. Systematic Titration Experiments. Stimulated by the experience with self-assembled multipophyrin arrays, we have varied steady state experiments on YQD (and to a less extent on RQD) systematically by using a series of differently substituted H_2P porphyrins (see Scheme 1). The strategy was to vary (i) the number of pyridyl-rings from 1 to 4 including the two variants (m-Pyr)$_2$H$_2$P and ($m\wedge$Pyr)$_2$H$_2$P, in which the pyridyl rings are opposite or adjacent to each other. We replaced (ii) the type of nitrogen (N) position within the pyridyl ring from the meta- to ortho- and para-N position in the case of the 4-fold pyridyl-substituted H_2P molecules. Finally (iii), we replaced the solvent toluene with chloroform and used the more spacious but better soluble isopropyl−phenyl-substituted pyridyl porphyrins (see Scheme 1) in some cases. In a control experiment, we added pyridine in comparable molar concentrations as we did for H_2P, which, however, did not result in a noticeable quenching of the PL of YQD at these low pyridine concentrations.

The most pronounced effects on YQD PL are observed upon changing the number and type of pyridyl substitution. As can be seen in Figure 5, such changes have a dramatic influence on the PL quenching of YQD. We define the relative quenching efficiency (E) by the PL intensity ratio

$$E = \frac{I(x)}{I(x=0)} = \frac{I(x)}{I(0)} \qquad (1)$$

The most obvious observation is that (o-Pyr)$_4$H$_2$P almost does not quench the QD PL, whereas the quenching is strongest for (p-Pyr)$_4$H$_2$P, which is followed closely by (m-Pyr)$_4$H$_2$P. Within the (m-Pyr)$_n$H$_2$P manifold, there is a systematic increase of the quenching efficiency on the number (n) of pyridyl substituents

TABLE 1: Nanoparticle Properties and FRET Parameters for QD-H_2P Arrays (toluene, 295 K, refractive index $n = 1.4969$)

QD-H_2P array	r_Σ,[a] Å	φ_D[b]	λ (nm)/ $\epsilon(10^3\,M^{-1}\,cm^{-1})$[c]	$J(\nu)$,[d] $10^{-14}\,cm^6\,M^{-1}$	R_0^{theor},[e] Å	R_{DA},[f] Å	τ_D^{0g}, ns	k_{DA},[m] $10^8\,s^{-1}$ (calcd)	τ_D^n, ns (calcd)
YQD + (*m*-Pyr)$_3$$H_2P$	22.5	0.53	515/19.7	7.95	39.0	28.1	15[j]	5.45	1.8
YQD + (*m*-Pyr)$_4$$H_2P$	22.5	0.5	516/19.3	7.94	38.9	28.1	15[j]	4.72	2.1
RQD + (*m*-Pyr)$_3$$H_2P$	31.0	0.41	515/19.7	3.85	33.1	36.6	20[k]	0.27	37.1

[a] An overall core−shell radius of CdSe/ZnS quantum dot was calculated by $r_\Sigma = d(CdSe)/2 + nl$ where d is QD diameter and l is the thickness of one ZnS layer. [b] φ_D is the experimentally measured QD photoluminescence quantum efficiency. [c] Wavelength (λ) of acceptor (porphyrin) absorption maximum and the corresponding molar decimal extinction coefficient (ϵ). [d] $J(\nu) = \int_0^\infty f_D(\nu)\epsilon_A(\nu)\frac{d\nu}{\nu^4}$ is the overlap integral between the donor (QD) emission and the acceptor (H_2P) absorption.[85] [e] $R_0^{theor} = \frac{9000\ln 10 k^2 \varphi_D^0}{128\pi^5 n^4 N_A} \times \int_0^\infty f_D(\nu)\epsilon_A(\nu)\frac{d\nu}{\nu^4}$ is the critical Foerster FRET radius,[47,48] N_A is Avogadro's number, and the orientational factor $\langle\kappa^2\rangle = 0.476$ for rigid random distribution of interacting dipoles. [f] For a two-point interaction of the H_2P molecule with the QD surface, the intercenter distance was estimated for the (*m*-Pyr)$_3$$H_2P$ and (*m*-Pyr)$_4$$H_2P$ optimized structures by $R_{DA} = r_\Sigma + [r_m^2 - (h/2)^2]^{1/2}$, where $r_m = 7.55$ Å is the radius of the porphyrin molecule with opposite pyridyl rings having nitrogens in meta positions and $h = 10$ Å is the mean distance between the meta nitrogens of adjacent pyridyl rings (HyperChem software, release 4.0 geometry optimization with semiempirical PM3 method, see Scheme 1). [g] τ_D^0 corresponds to the intrinsic PL of CdSe QD. [j] Estimated according to RQD decay shortening observed upon shifting the detection wavelength to the blue. [k] Experimental τ_D^0 value measured by the TCSPC method. [m] FRET rate constant, according to eq 8. [n] QD decay shortening $\tau_D = 1/[(1/\tau_D^0) + k_{DA})]$.

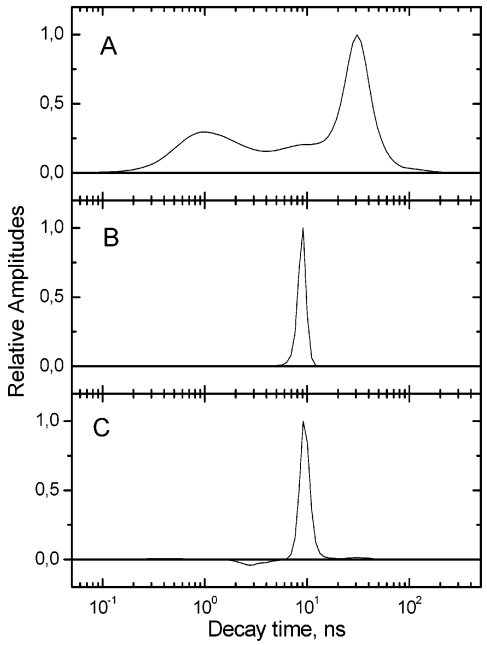

Figure 4. Decay amplitude distributions for RQD (A), (*m*∧Pyr)$_3$$H_2P$ (B) and RQD + (*m*Pyr)$_3$$H_2P$ at a molar ratio of $x = 4.5$ (C) (λ_{exc} = 575 nm, λ_{em} = 650 nm).

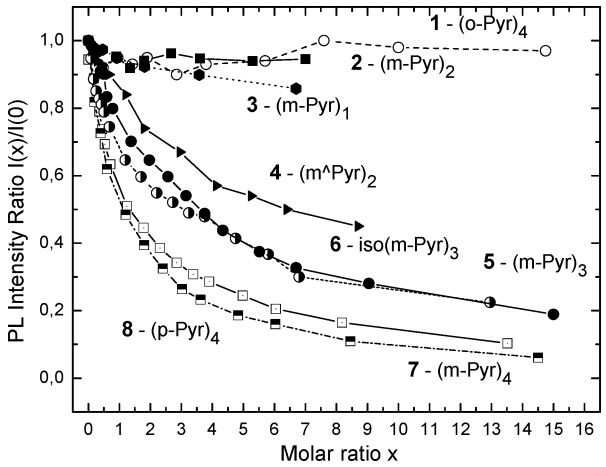

Figure 5. PL intensity ratio $E = I(x)/I(0)$ for YQD as a function of the molar ratio (x) and various porphyrin molecules. 1 (- -○- -) - (*o*-Pyr)$_4$$H_2P$; 2 (−■−) - (*m*-Pyr)$_2(Ph)_2$$H_2P$; 3 (···●···) - (*m*-Pyr)$_1$$H_2P$; 4 (−▼−) - (*m*∧Pyr)$_2$$H_2P$; 5 (−●−) - (*m*-Pyr)$_3$$H_2P$; 6 (- - -◑- - -) - (iso)-(*m*-Pyr)$_3$$H_2P$; 7 (−□−) - (*m*-Pyr)$_4$$H_2P$; 8 (-·-·-■-·-·-) - (*p*-Pyr)$_4$$H_2P$.

when changing from (*m*-Pyr)$_1$ to (*m*-Pyr)$_4$. The only exception refers to opposite (*m*-Pyr)$_2$$H_2P$, which shows an overall behavior more similar to (*m*-Pyr)$_1$, whereas adjacent (*m*∧Pyr)$_2$$H_2P$ shows a much more efficient quenching similar, for example, to (*m*-Pyr)$_3$$H_2P$. The influence of isopropyl groups (compare curves 5 and 6 in Figure 5) or the solvent chloroform as compared to toluene is of minor importance.

It has to be mentioned that PL quenching such as that shown in Figure 5 is qualitatively the same in all series of the experiments we have performed so far for QD samples including those from different sources. Quantitatively, there will be, however, changes from sample to sample indicating that other processes depending on TOPO and/or the ZnS shell influence the quenching mechanism or the for self-assembling dynamics. Also, additional constituents in the solvent might influence the quantitative behavior of the QD-H_2P nanoassemblies' photoluminescence. Especially, the quenching efficiency at high molar concentrations, that is, the maximum obtainable quenching efficiency, is sensitive to sample preparation and storage. In some cases, we have observed quenching efficiencies for (*p*-Pyr)$_4$$H_2P$ of nearly 100%. Additional evidence for (unknown) sample variations stems from the temperature dependence of the QD PL. Upon a temperature increase from 295 to 355 K and decrease to 255 K, the PL decreases (partly irreversible) even without the presence of H_2P. A maximum PL is observed at about 273 K, possibly indicative of freezing of water contamination. In this respect, it should be mentioned that other environmental effects (e.g., oxygen) are also discussed in the literature.[44]

To test the stability of the obviously formed QD-H_2P assemblies, we have added pyridine or acetone to the solution (Figure 6). Pyridine has been used because it also may form complexes with CdSe/ZnS nanocrystals.[41] As was shown in our previous studies on multipophyrin arrays,[7,25,26] it was possible to break up these organic complexes while adding pyridine as a competitive complex formation channel. In the case of QD-H_2P assemblies, as shown in Figure 6, for samples containing only YQD, the increase of pyridine in large amounts (up to 22 vol % of toluene) results in a reduction of the YQD PL relative intensity down to $E \approx 0.1$ (curve 2). In contrast, adding the same amount of pyridine to a sample containing both YQD and H_2P at $x = 4.7$, we get an (additional) quenching of only $E \approx 0.25$ (curve 1).

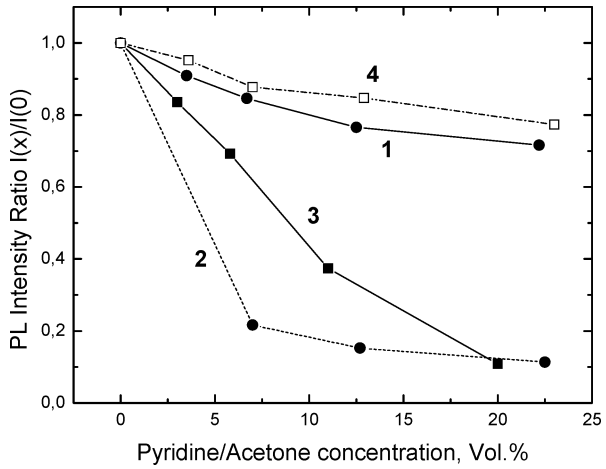

Figure 6. Photoluminescence intensity ratio $E = I(x)/I(0)$ of YQD as a function of added pyridine (1; 2) and acetone (3; 4) in vol % of toluene with (1; 3) and without (2; 4) (*m*-Pyr)$_3$H$_2$P at a molar ratio of $x = 4.7$.

Acetone, however, is a much more polar solvent than toluene, thus possibly influencing solvation and/or charge-transfer dynamics, which are generally fastened upon increasing polarity.[45] The data presented in Figure 6 show that for a sample containing only YQD, we observe a PL quenching of about $E \approx 0.8$ at an acetone volume ratio of 23% (curve 4), whereas in the presence of H_2P at $x = 4.7$, the quenching is enhanced, resulting in $E \approx 0.1$ (curve 3).

Inspecting various H_2P fluorescence spectra, we always observe, as shown in Figure 2, a spectral red shift by about 2 nm (at maximum) upon H_2P concentration increase. At H_2P concentrations at which almost no changes in the quenching efficiencies (E) are observed, the red shift no longer proceeds though the H_2P and the fluorescence intensity is still increasing nearly linearly. The fluorescence spectra at high x values resemble those of uncomplexed H_2P molecules, as is also evident from Figure 2. Also, a change of the Franck−Condon envelope (as manifested by a variation of electronic and vibrational band relative intensities) is observed. The origin of the blue shift of the H_2P fluorescence upon anchoring to the QD surface (at low concentrations) with respect to uncomplexed H_2P remains unexplained. The manifestation of spectral shifts as a function of the molar ratio (x) indicates that at low x values, H_2P molecules are (partly) complexed with QD resulting in a spectral blue shift, whereas a further H_2P concentration increase above a "critical" concentration of about $x = 4$ merely results only in "free" H_2P entities. Noteworthy, in the solutions under study, the porphyrin absolute concentrations ($C_{porph} \approx (8 \times 10^{-6})/(4 \times 10^{-5}$ M)) are still far below the aggregation effects known for H_2P molecules. Similar spectral shifts have also been observed upon complex formation of H_2P with Zn-porphyrin chemical dimers.[7,25,26] In that case, the (red) shift has been attributed to an overlap of π orbitals of interacting tetrapyrrolic macrocycles. According to our measurements, the fluorescence quantum efficiency (φ) and the fluorescence decay time (τ) for complexed H_2P molecules remain almost the same as those for uncomplexed H_2P, although a small deviation from linearity has been observed for the H_2P fluorescence intensity rise upon increasing the molar ratio (x) (see Figure 7A, curve 2).

The fluorescence excitation spectra of H_2P provide information about a possible fluorescence resonant energy transfer (FRET) from CdSe/ZnS to H_2P. Unfortunately, a direct fluorescence excitation spectrum always contained CdSe/ZnS

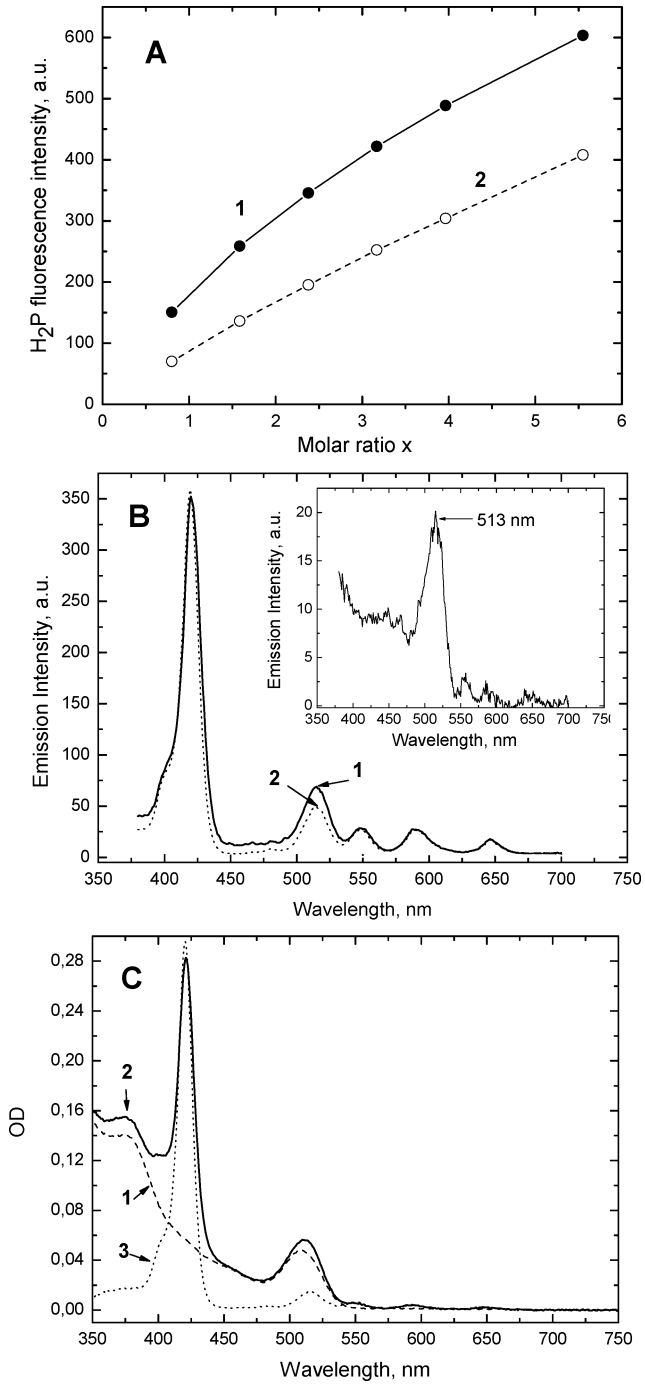

Figure 7. Fluorescence enhancement of (*m*-Pyr)$_4$H$_2$P upon excitation of YQD. (A) Porphyrin fluorescence intensity increase (λ_{em} = 651 nm) as a function of x: (1) λ_{ex} = 465 nm, YQD excitation; (2) λ_{ex} = 590 nm, (*m*-Pyr)$_4$H$_2$P excitation. The normalization procedure is described in the text. (B) Fluorescence excitation spectra for (*m*-Pyr)$_4$H$_2$P fluorescence Q(0, 1) band (λ_{em} = 720 nm): (1) YQD + (*m*-Pyr)$_4$H$_2$P at $x = 0.8$; (2) (*m*-Pyr)$_4$H$_2$P at $x = 0.8$. The inset of Figure 2B presents the difference spectrum ((1) − (2)) with a maximum at 513 nm, which is characteristic for YQD absorption. (C) Comparative absorption spectra for YQD (1), YQD + (*m*-Pyr)$_4$H$_2$P at $x = 0.8$ (2) and (*m*-Pyr)$_4$ H$_2$P (3) at the same molar concentration as in (2).

absorption bands because the emission in the H_2P fluorescence detection wavelength range ($\lambda_{em} \geq 720$ nm) was always superimposed by the remaining CdSe/ZnS PL, which embarrasses an unique identification of the excitation routes. Therefore, we have corrected, as a function of x, all of the H_2P excitation spectra for the remaining QD PL at 720 nm, assuming a linear superposition of PL of QD and H_2P while taking into

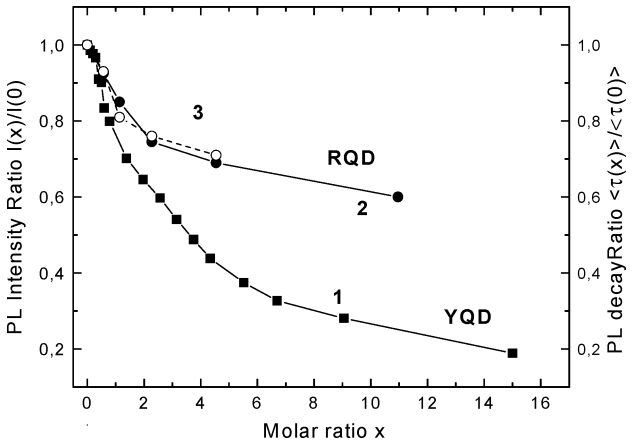

Figure 8. PL intensity ratio $E = I(x)/I(0)$ as a function of the molar ratio (x) for YQD + (m-Pyr)$_3$H$_2$P ($\lambda_{ex} = 465$ nm, $\lambda_{em} = 524$ nm) (1), and RQD + (m-Pyr)$_3$H$_2$P ($\lambda_{ex} = 465$ nm, $\lambda_{em} = 585$ nm) (2). (3) Relative PL decay ratios $\langle\tau(x)\rangle/\langle\tau(0)\rangle$ determined from PL decays as weighted mean lifetimes $\Sigma(f_i\tau_i)/\Sigma(f_i)$ for RQD without ($\langle\tau(0)\rangle$) and with (m-Pyr)$_3$H$_2$P ($\langle\tau(x)\rangle$) ($\lambda_{ex} = 575$ nm, $\lambda_{em} = 585$ nm).

account the proper QD PL quenching at a given molar ratio (x). The via QD absorption mediated fluorescence excitation spectrum for H_2P (inset of Figure 7B) has been obtained while subtracting the excitation spectrum of a pure H_2P solution (at the same concentration and calibrated at 590 nm) from the H_2P fluorescence excitation spectrum in the presence of YQD. The difference spectrum clearly shows a YQD absorption band at $\lambda_{max} = 513$ nm.

By monitoring the H_2P fluorescence intensity at $\lambda_{em} = 651$ nm as a function of x and comparing the results obtained for excitation wavelengths either at the QD absorption band at 465 (YQD) or 575 nm (RQD), respectively, or via direct excitation into the H_2P Q-band absorption at 590 nm, we showed that the H_2P fluorescence increase with x is more pronounced (enhanced) for QD excitation than for direct H_2P Q-band excitation at the same wavelength (corrected for the spectral response). These observations clearly show the existence of a fluorescence enhancement effect (FRET) for H_2P molecules anchored on QD (Figure 7A and B).

Finally, Figure 8 shows a comparison of the PL quenching for YQD ($d = 2.5$ nm; two ZnS monolayers) and RQD ($d = 3.2$ nm; three ZnS monolayers) upon titration by (m-Pyr)$_3$H$_2$P. The quenching efficiency is evidently stronger for YQD at comparative molar ratios (x). Noteworthy, the quenching efficiency for RQD determined from these static experiments is in satisfying agreement with the one deduced from the decay component analysis obtained from time-resolved experiments (see Figure 3). In Figure 8, we have additionally plotted the normalized sum of the decay amplitudes

$$\frac{\sum_i (f_i\tau_i)}{\sum (f_i)}$$

where f_i is the relative amplitude of the decay component, τ_i.

4. Discussion

In the present publication, we will concentrate on the building principles of nanoassemblies (section 4.1) and the related photoluminescence quenching efficiencies (section 4.2), whereas the identification of the quenching mechanisms is considered to be qualitative and will need future experiments.

4.1. Formation and Structure of Nanoassemblies. The observed PL quenching of CdSe/ZnS in combination with the time-resolved PL decay and the H_2P fluorescence enhancement is a clear indication that QD and H_2P are in close spatial proximity to each other despite the extremely low concentrations used in the experiments. The quenching is a manifestation of an effective electronic interaction, for example, via charge or excitation energy transfer between the constituents of the nanoassembly. The results in Figure 5 clearly prove that functionalization of the H_2P molecule by mesopyridyl groups changes the degree of QD PL quenching systematically and thus provides information on both the mechanism of the complex formation and the structure of the self-assembled complexes. Because the titration by nonfunctionalized H_2P does not lead to any noticeable quenching effects, it is obvious that pyridyl substituents play a crucial role in the QD-H_2P formation process. If, however, adding pyridine, the molecular ligating analogue of pyridyl, in comparable molar ratios, as was done for H_2P, no PL quenching of QD is observed (see Figure 6). The results presented in Figures 5 and 6 thus prove that the QD PL quenching is related to the anchored porphyrin macrocycle and not merely the pyridyl constituent. Only at much higher pyridine concentrations of small volume percents (curve 1, Figure 6), the YQD PL is quenched, as has been reported recently[41] for other CdSe/ZnS systems. In those cases, the effect has been related to the exchange of the TOPO shell by pyridine.[41]

From this comparison, we conclude that pyridyl substituents exhibit a functional role similar to that in the formation of multichromophoric porphyrin arrays,[7,25,26] namely, the formation of complexes. The chemical reason for complex formation is the capability of the pyridyl nitrogen lone pair orbital to form bonds with, for example, Zn-porphyrins central ions or the ZnS shell of the CdSe/ZnS nanocrystals. Several experiments have been reported that also prove that functionalized dye molecules[16−18] and biomolecules[19−22] assemble on semiconductor quantum dot surfaces.

In the present case, we demonstrate for the first time a systematic investigation on the structure and formation dynamics of assemblies that are formed from quantum dots and dye molecules. For recently reported porphyrin arrays, we have proven that allosteric effects result in a key-hole principle of matching nitrogen−nitrogen separations with those of the Zn−Zn distance.[7,25,26] However, such selective principles are not to be expected for the formation of the currently reported hybrid nanoassemblies because the surface of the QD is large compared to nitrogen−nitrogen distances in pyridyl-substituted H_2P molecules, thus offering multiple possibilities for anchoring porphyrins on the CdSe/ZnSe surface. This argument holds under the assumption that there is a large number of coordination points for a nitrogen lone pair interaction on the relevant surface. In principle, the number of coordination points is comparable to the one which governs the coordination of TOPO molecules. From literature,[32] it is known that the percent coverage of TOPO on CdSe nanocrystals decreases as the QD radius increases, reaching a saturation coverage of ~20%. It follows from the radius dependence of the TOPO coverage for CdSe QD[32] that for YQD ($d = 2.5$ nm) and RQD ($d = 3.2$ nm) the percent coverage is estimated to be 35 and 30%, respectively. Assuming uniform surface coverage, the number of TOPO molecules per unit surface area of CdSe QD has been estimated[35] to be ~10 nm^{-2}, whereas pyridine exchanges TOPO up to about 12% coverage.[32]

When comparing the quenching efficiency for various tetrapyridyl H_2P molecules, the quenching efficiency for ortho compounds (see Scheme 1) is almost negligible (see Figure 5, curve 1) with respect to meta and para variants (curves 7 and 8). For para variants, we always observed slightly higher quenching efficiencies as compared to meta variants. According to geometric reasons in the case of the ortho variant, an anchoring of the nitrogen lone pair orbitals can occur only for an orientation of the porphyrin macrocycle nearly parallel to the QD surface. From the absence of QD PL quenching in the latter case, we conclude that despite the flexibility of pyridyl rings with respect to the H_2P macrocycle, a parallel orientation of the macrocycle with respect to the QD surface is obviously not favored. However, an orientation of the porphyrin macrocycle nearly perpendicular to the QD surface would be easily possible for meta and para variants of H_2P molecules.

A further variation of interaction geometries is related to the number of pyridyl rings per H_2P molecule. For this reason, we have investigated a whole series of metapyridyl-substituted compounds (see Scheme 1). As can be seen from Figure 5, the QD PL quenching efficiency for a given molar ratio (x) decreases while decreasing the number of pyridyl rings. Moreover, for the (m-Pyr)$_2$H$_2$P molecule with opposite pyridyl rings, the quenching efficiency is more similar to that found for a (m-Pyr)$_1$H$_2$P molecule with only one pyridyl ring, whereas the quenching is essentially stronger for ($m\wedge$Pyr)$_2$H$_2$P molecules having two adjacent pyridyl rings. From these combined observations, we conclude that H_2P molecules anchor on the CdSe/ZnS surface in a nearly perpendicular fashion with two nitrogen lone pair orbitals (at most) forming coordination bonds with the surface. From geometric arguments, the QD PL weak quenching behavior observed for H_2P molecules with opposite pyridyl rings can thus be easily rationalized because a contact of opposite pyridyl rings to the surface is impossible due to geometric reasons in the case of a perpendicular orientation of the porphyrin macrocycle with respect to the QD surface. As is also evident from Figure 5, the more spacious isopropyl groups (curve 6) do not influence the complexation considerably.

Thus, with respect to the QD surface, the overall structural model for the QD-H_2P nanoassembly is a nearly perpendicular orientation of the porphyrin macrocycle with two lone-pair coordination contacts at most. Considering space-filling molecular entities for such nanoassemblies, one H_2P molecule replaces about two TOPO molecules or, alternatively, fills a free volume corresponding to two TOPO molecules. The overall information is shown schematically in Figure 9 nearly on scale for the two types of QD reported in this paper.

As shown in Figure 5, the QD PL quenching efficiency and thus the probability to form QD-H_2P nanoassemblies is decreased with a decreasing number of pyridyl rings. Assuming that the probability to form an assembly is linearly proportional to the number of pyridyl rings, we can define an effective molar ratio $x_{pyr} = x(^N/_4)$ that scales with N, where N is the number of pyridyl rings for a given H_2P molecule. Correspondingly, x_{pyr} becomes smaller with a decreasing number of pyridyl rings. Doing so, we obtain a rescaling of the QD PL quenching efficiency for every H_2P molecule, as depicted in Figure 10. In the result, all of the quenching curves besides those for (m-Pyr)$_1$H$_2$P, (m-Pyr)$_2$H$_2$P, and (o-Pyr)$_4$H$_2$P are shifted toward one single curve. The overall result is a kind of "master" curve for the quenching efficiency. In case that only one pyridyl ring can be anchored effectively, the agreement with the master curve becomes less satisfactory. From this behavior, we conclude that

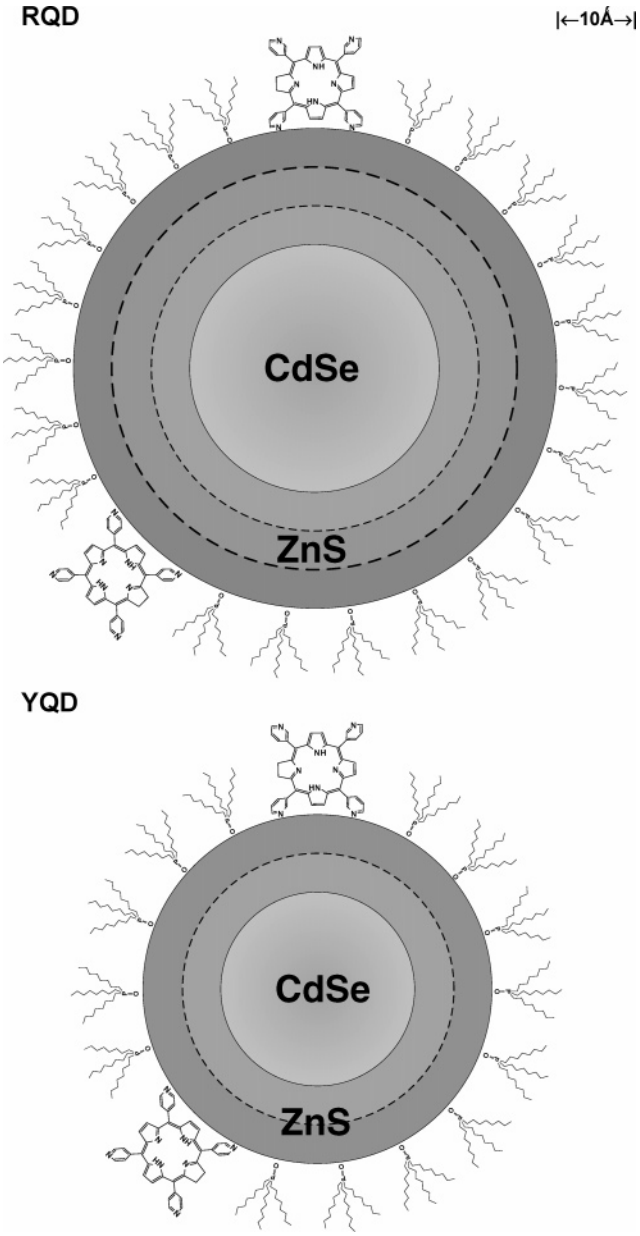

Figure 9. Schematic presentation of QD-H_2P arrays. The scales of the CdSe core, ZnS shell, porphyrin and TOPO molecules as well as intercenter distances correspond to the relative sizes of the main components of the arrays.

our assumption relating the probability to form a complex with the number of pyridyl rings having access to the QD surfaces is correct. The stability of a two-point interaction will be at least a factor of 2 stronger than a one-point interaction, as can be deduced from the pronounced mismatch of the (scaled) one-point interaction curves for (m-Pyr)$_1$H$_2$P and (m-Pyr)$_2$H$_2$P as compared to the master curve. The importance of a two-point interaction has also been demonstrated for CdSe/ZnS QD-protein complexes.[46]

The variation of the QD PL quenching efficiency with respect to the number, kind, and position of pyridyl rings in H_2P molecules points toward a dynamic equilibrium between nanoassemblies and free entities, as has also been observed for multiporphyrin arrays.[7,25,26] The equilibrium is dynamic, assuming an infinitely strong coupling would not result in a dependence of the quenching on the number of pyridyl rings. An analysis of this dynamic equilibrium will be discussed in

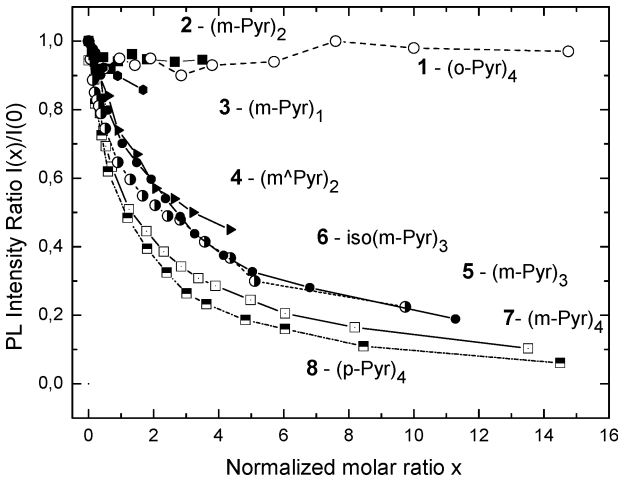

Figure 10. PL intensity ratio $E = I(x)/I(0)$ for YQD as function of the (to the number of pyridyl groups) normalized molar ratio (x) and various porphyrin molecules. 1 (- -○- -) - (o-Pyr)$_4$H$_2$P; 2 (−■−) - (m-Pyr)$_2$(Ph)$_2$H$_2$P; 3 (⋯●⋯) - (m-Pyr)$_1$H$_2$P; 4 (−▼−) - (m∧Pyr)$_2$H$_2$P; 5 (−●−) - (m-Pyr)$_3$H$_2$P; 6 (- - -◑- - -) - (iso)(m-Pyr)$_3$H$_2$P; 7 (−□−) - (m-Pyr)$_4$H$_2$P; 8 (-•-•-■-•-•-) - (p-Pyr)$_4$H$_2$P.

the following section (4.2) with respect to the quenching efficiency as a function of the molar ratio (x).

4.2. Photoluminescence Quenching Efficiency. After having established that PL quenching observed for QD is due to the formation of specific nanoassemblies formed from QD and H_2P molecules, we will outline the general formalism of the PL quenching without considering the concrete quenching mechanism that will be postponed to the subsequent section (4.3).

In the previous section, we showed that with an appropriate H_2P pyridyl substitution, QD-H_2P nanoassemblies can be formed in a dynamic equilibrium. Because QD are, in principle, capable to "host" (as has also been shown in other cases[16,19]) more than one H_2P molecule, the equilibrium cannot be described by the scheme of a bimolecular reaction as has been done previously for multiporphyrin assemblies.[7,25,26] Instead, as the simplest variant, we have to consider a Poisson distribution for nanoassemblies supposing an independent interaction of every H_2P molecule with a given QD.

As the formation of nanoassemblies becomes evident via the QD PL quenching, there should be mechanisms such as charge or excitation energy transfer between the entities of the assembly. Independent of the nature of the concrete mechanism or combinations of them, the QD PL quenching can be modeled by introducing a quenching rate constant $k_Q = k_{CT} + k_{ET}$, which characterizes a competitive decay channel with respect to the intrinsic CdSe/ZnS PL decay described by the rate constant k^r. Here, we have assumed that the k_{CT} and k_{ET} rate constants represent photoinduced charge transfer and energy transfer processes, respectively. For the sake of simplicity, we assume that the observed distribution of decay rate constants of QD PL is due to a distribution of (unknown) assemblies and not a dynamic inhomogeneity for a single nanoassembly, although the letter process will basically not render our considerations.

In principle, all QD PL decays characterized by the observed distribution of decay times should be shortened additionally in the case of anchored H_2P molecules (the corresponding rate constant is k_Q). Correspondingly, such a shortening and thus quenching of PL will only show up in the experiment if the k_Q value becomes comparable to the relevant intrinsic (though unknown) decay rate constants. However, as seen from Figure 3B, the fast decay components only contribute partly to the steady state PL intensity, which is determined predominately by the intrinsic (radiative) decay rate constant, $k^r \approx (20\ \text{ns})^{-1}$. A direct comparison of steady-state and time-resolved PL quenching has only been performed systematically for RQD (see Figure 8), but we have evidence that a similar behavior is present in most of our investigated samples.

At a given excitation intensity, the related QD PL intensity $I(0)$ at $x = 0$ is proportional to the QD PL quantum efficiency

$$\varphi_D = \frac{k^r}{k^r + \sum_i k_i^{nr}} \tag{2}$$

where k^r corresponds to the intrinsic radiative rate constant and k_i^{nr} corresponds to the intrinsic nonradiative decay rate constants, respectively. In case that the QD PL is quenched additionally by external mechanisms (e.g., while varying the concentration (x) of an added quencher) the apparent quantum efficiency (φ) will be further reduced, resulting in a relative QD PL quenching efficiency

$$E = \frac{I(x)}{I(o)} = \frac{(k^r + \sum_i k_i^{nr})}{(k^r + \sum_i k_i^{nr} + \sum_j n_j k_{Qj})} \tag{3}$$

where k_{Qj} is the quenching rate constant related to the quenching process j and n_j is the number of quenchers per QD and per process j. Replacing for simplicity $(k^r + \sum_i k_i^{nr})$by k_D and assuming only one additional quenching process ($j = 1$), eq 3 becomes, at a given molar ratio (x),

$$E(x) = \frac{k_D}{k_D + n k_Q} \tag{4}$$

where k_D is the total QD decay rate constant and k_Q is the quenching rate constant, respectively. In case that x is given as the molar ratio x_M per QD, n becomes equal to x_M. This formula has, for example, been applied recently[19] to describe FRET processes from a series of QD to a well-defined number (n) of attached dye molecules per QD.

In the present situation in which QD PL quenching is caused by the titration of QD at a fixed concentration by a variable concentration of H_2P molecules, the simple approach outlined above has to be modified because the interacting components of the respective H_2P-QD nanoassemblies are in a dynamic equilibrium with each other. Opposite of a bimolecular complex formation, for example, observed in a series of experiments on multiporphyrin arrays,[7,25,26] we have to assume that more than one H_2P molecule might be (dynamically) attached to the surface of a single QD. In the presented experiments, QD PL is recorded within about 120 s after a titration step. Because we observe only small (less than additional 5%) changes in the PL on a time scale of a few hours after a titration step, we have to assume that dynamic equilibrium is reached in less than 60 s at the concentrations used in the experiment. However, we would like to mention that we have observed further QD PL changes (depending on titration steps and sample preparation techniques) on time scales longer than 24 h, indicating a reorganization of the assemblies (which probably includes rearrangements of the TOPO shell). These effects showing up noticeably only at times much longer than 3 h have been ignored in this paper but are currently under more detailed investigation.

With the assumption that the quenching H_2P molecules anchor on the QD surface independently of each other, the probability $P(n, x)$ to find molecules fixed on the surface at a given molar ratio (x) is described by the Poisson distribution

$$P(n, x) = x^n \frac{\exp(-x)}{n!} \quad (5)$$

where $n = 0-\infty$. This equation holds in the case that the complexation constant (K) is infinitely large, which implies that we do not have to consider a dynamic equilibrium. Under these conditions, n becomes equal to x_{eff}. As will be shown elsewhere, the necessity to apply such a distribution instead of eq 4 depends drastically on the ratio k_D/k_Q. As will be discussed later in this report, $k_D/k_Q > 1$ and we may use eq 4 safely.

Two remarks have to be made. First, because we are dealing with nanocrystals, only a limited number of H_2P molecules can be assembled on the accessible surface area.[32,35] However, the maximum number (n_{max}) of anchored H_2P molecules will depend on several factors, for example, the number and kind of "vacancies" (accessible places on the QD surface which are not occupied by TOPO molecules) as well as the competitive dynamic equilibrium between TOPO and H_2P molecules depending on both complexation constants for TOPO and H_2P and their relative concentrations. Because we do not have experimental access to these parameters currently, we will assume no limitations to n_{max} in this publication. Second, besides H_2P quenchers, there might be additional unknown quenchers present in our samples that show up in a nonexponential decay of the QD PL already in the absence of H_2P (see Figure 3). Similar observations have also been reported in several publications.[38,42] To include these aspects in eq 4 is far beyond the scope of the present publication, and we will need more detailed time-resolved experiments, which are under investigation currently. In the following, we will therefore assume that the main quenching effects are due to the quenching processes of those QD that are not yet quenched by other (unknown) processes. It will turn out that this procedure is justified by our experimental findings.

The experimental data for the quenching efficiency $E = I(x)/I(0)$ shown in Figure 10 as a function of the rescaled molar ratio (x) demonstrate that nk_{Qj} is approximately the same for most of the arrays based on YQD. This implies that all of the variants of pyridyl-substituted H_2P molecules exhibit the same quenching mechanism upon assembling on the YQD surface and differ mainly in the $x_{\text{eff}} = x_{\text{pyr}}$ values. Additional supporting information is provided via time-resolved experiments on RQD-H_2P complexes. The time-resolved data for RQD can be compared to the corresponding (static) quenching efficiency. Figure 8 demonstrates that RQD PL quenching detected by decay analysis or static PL quenching experiments are in agreement with each other.

We calculate the expected quenching efficiency, $E = I(x)/I(0)$, under the assumption that the experimentally given molar ratio (x) corresponds to x_{eff} and that one H_2P molecule per QD is sufficient to significantly quench PL of the given QD and thus remove this QD-H_2P complex from the (intrinsic) decay component of 20 ns. With this assumption, the intrinsic decay component of RQD should be reduced independently of the absolute value of the quenching rate constant. This opens the possibility to approximate x_{eff} by adjusting the PL decay component at $\tau \approx 20$ ns to the experimentally observed one via the relation $I(x) = I(0)\cdot\exp(-x/p)$, where p is given by $p = x/x_{\text{eff}}$. The corresponding fitting procedure is shown in Figure 11 as an inset and results in $p = 10$. This implies that the nominal molar ratio (x) has to be reduced to an effective ratio of $x_{\text{eff}} = x/10$. From this, we conclude that either the dynamic equilibrium in the assemblies does not favor a strong complexation of H_2P molecules on the surface of a QD or that there is only a limited number of accessible sites on the QD surface. With this result, the number (n) in eqs 3 or 5 should be reduced to $n = x_{\text{eff}} \approx 0.1x$.

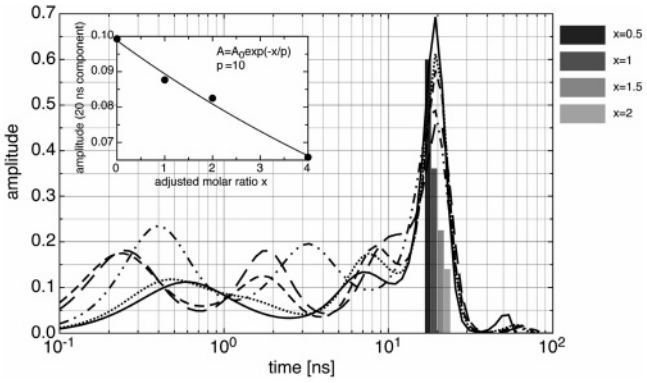

Figure 11. PL decay components of RQD at various x values and a fit (inset) of the intrinsic component at $\tau \approx 20$ ns assuming complexation of RQD. Bars indicate calculated intensity assuming that each H_2P is complexed with RQD.

The question remains whether the observed reduction of x to x_{eff} is the consequence of a dynamic equilibrium or a limited number of accessible sites. There are some experimental observations that are in favor of limited sites. As shown in Figure 2, we observe a spectral red shift of H_2P fluorescence by about 2 nm upon increasing x. At molar ratios >5, this shift results in a spectrum that corresponds to the fluorescence spectrum of H_2P in the absence of QD. A further increase of H_2P will obviously only create free H_2P fluorescence, which is in contradiction with the assumption of a dynamic equilibrium involving an unlimited number or at least a large number (n_{max}) of accessible sites. The number of sites is, thus, lower at the relevant molar ratios than at the maximum statistical number of H_2P molecules on a given QD surface. However, we have determined, according to the quenching efficiency, that only $^1/_{10}$ of H_2P molecules are complexed with a QD. Can such a low concentration of complexed H_2P molecules per one QD result in an effective spectral shift as observed in Figure 2? To answer this question, one should consider that those QD that are already "quenched" intrinsically also have to be taken into account (see Figure 3). These QD may be complexed with H_2P without resulting in noticeably additional quenching. With respect to the H_2P fluorescence, this will, nevertheless, result in a shift of the H_2P fluorescence band. In conclusion, relating the quenching efficiency to the number of H_2P molecules requires a reduction of the initial molar ratio (x) by a factor of about 10. However, the presence of already quenched QD PL by unknown quenchers (see Figure 3), will increase the average number of H_2P molecules per QD. Combining these two observations results in a value of about $n > {}^1/_5$ H_2P molecule per QD. (Also see Table 1 for the experimentally determined PL quantum efficiency (φ_D) of QD, which brings QD PL quenching and fluorescence shifts of H_2P in reasonable agreement with each other.)

A final comment is related to the small time-resolved fluorescence build up of H_2P, which is shown in Figure 4. As we will show in the following chapter, the observed build-up time of 2−3 ns is much too fast to be explained by FRET from RQD to H_2P. However, even if this time is not related to a direct energy transfer process from QD to H_2P, it might nevertheless show up in the fluorescence increase of H_2P because, as we have discussed just before, H_2P will also be complexed to those RQD, which are already subject to PL

quenching. In this case, a fast (unidentified) quenching process might result in a subsequent population of H_2P.

4.3. Quenching Mechanisms. Until now, we have described the PL quenching of CdSe/ZnS upon titration by H_2P merely by a fictive quenching rate constant, k_Q (or to be more specifically $n \cdot k_Q$), without specifying any mechanism that causes this process. In fact, mainly two processes have to be considered, namely, (i) fluorescence resonant excitation energy transfer (FRET) from QD to H_2P and (ii) photoinduced charge transfer (CT) within the nanoassembly. FRET has been identified in numerous organic[47,48] and inorganic[49,50] materials and has also been reported for several QD-dye systems.[18,19] Photoinduced CT on the nanoscale has been observed in a variety of molecular arrays such as photosynthetic reaction centers in vivo,[51] porphyrin assemblies,[6,7,26,45,52] and nanoparticle-dye heterostructures.[16,17,45] Many experiments on single semiconductor nanocrystals demonstrate photoinduced charge separation on long time scales.[53−56]

In the following, we would like to discuss some qualitative aspects of FRET as one of the quenching mechanisms in somewhat more detail, and we would like to work out that FRET experiments can be discussed as a tool to identify features of the formation of QD-H_2P nanoassemblies. However, we will not attempt to give a unique description of energy transfer processes in the nanoassemblies.

Fluorescence resonant energy transfer (FRET) has been described by Förster[47] (point dipole approximation) and Dexter[57] (exchange resonant interaction) and has been extensively investigated. The Förster-type model describes the nonradiative energy transfer between weakly interacting chromophores (e.g., from a photoexcited donor (D) to an acceptor (A)).

The application of the Förster theory[47] relies on the approximation that the intercenter distance, R_{DA}, between interacting dipoles of D and A is larger than the effective lengths of the donor and acceptor transition dipoles themselves. For absorption Q bands of various porphyrins, the effective lengths of the transition dipoles were estimated[7,26] to be $|l| \leq 1.0-1.3$ Å. However, the oscillator strength of QD low-energy excitonic transitions may be approximated as

$$f = 4.33 \times 10^{-9} \epsilon_{max}(\nu) \Delta\nu_{1/2} \tag{6}$$

where ϵ_{max} (ν) is the molar decimal extinction coefficient at the maximum of the excitonic absorption band and $\Delta\nu_{1/2}$ is the corresponding spectral halfwidth. Making use of the experimental data, we obtain $f = 0.3$ for YQD and $f = 0.55$ for RQD. The corresponding transition dipole moment, $|\mu|$, may be derived from the well-known expression

$$f = \frac{(8\pi^2 m_e \nu |\mu|^2)}{3he^2} \tag{7}$$

where ν is the transition frequency and m_e and e are electron mass and charge, respectively. Calculated values ($|\mu|$) become 6.9 D for YQD and 9.7 D for RQD, which is in reasonable agreement with the value 4.4 D, as calculated[49] for CdSe QD with diameters (d) of 22−44 Å. Correspondingly, this results in an effective dipole length ($|l|$) of 1.4 Å for YQD and 2.Å for RQD.

Assuming a perpendicular orientation of H_2P molecules on the QD surface as discussed in section 4.1, the intercenter distance (R_{DA}) becomes 28.1 Å for YQD and 36.6 Å for RQD. Even when assuming that the exciton is localized on the QD surface the estimated minimal D−A distances become at minimum 15.7 Å for YQD and 20.7 Å for RQD (see Table 1 and Scheme 1). From this, we conclude that R_{DA} is essentially larger than $|l|$ for both H_2P molecules and QD. This implies that in the case of QD-H_2P nanoassemblies the point dipole−dipole approximation is still valid. Finally, it should be mentioned that recent experimental results suggest that tightly bound nanocrystalline materials (QD−QD energy transfer[49,50]) and organic−inorganic hybrids[18,58] are best described in the weak coupling regime.

The FRET rate constant, k_{DA}, for an isolated D−A pair at the intercenter distance, R_{DA}, is expressed according to the Förster formalism[47] as

$$k_{DA} = \frac{1}{\tau_D^0} \frac{R_o^6}{R_{DA}^6} \tag{8}$$

where τ_D^0 is the D excited-state lifetime ($1/\tau_D^0 = k^r$) and R_0 is the critical Förster radius. As was discussed above, we define the distance R_{DA} by the distance from the center of the QD to the center of H_2P molecule. Obviously, R_{DA} depends on the type of QD including core diameter and ZnS shell thickness. An important parameter controlling FRET is, besides the distance R_{DA}, the overlap integral ($J(\nu)$) between the donor (QD) PL and the acceptor (H_2P) absorption spectra. Noteworthy, because of the quantum size effect, $J(\nu)$ values depend on the QD core diameter (d). The calculated and experimentally determined parameters relevant for FRET are collected in Table 1. From this, it is evident that for a given QD the overlap integral ($J(\nu)$) is almost independent of the type of the specific H_2P molecule being attached. It should be mentioned, however, that FRET might be in a competition with other photoinduced processes such as charge transfer.[59]

Currently, we do not have time-resolved photoluminescence data for all of our systems, but it is possible to estimate FRET efficiencies via the sensibilization of the H_2P emission (fluorescence enhancement). The FRET efficiency is given[19,48] by

$$E_{FRET} = \frac{[\epsilon_A(\lambda_{ex})F_{AD} - F_A]}{[\epsilon_D(\lambda_{ex})F_A n]} \tag{9}$$

where F_{AD} corresponds to the H_2P (acceptor) fluorescence intensity measured at λ_{em} (e.g., 651 nm for H_2P) while exciting at the donor absorption ($\lambda_{ex} = 465$ nm for YQD). F_A corresponds to the H_2P emission (in the absence of the QD donor) at the same concentration as in the former case and the same experimental (λ_{em}, λ_{ex}) conditions. n corresponds to the number of A molecules per donor D. We assume that at a given molar ratio (x), RQD and YQD have a similar number of H_2P molecules anchored on the QD surface. ϵ_A and ϵ_D correspond to the molar extinction coefficients of A and D, respectively, at the excitation wavelength λ_{ex}. At $\lambda_{ex} = 465$ nm (absorption exciton band for YQD) the ratio ϵ_A/ϵ_D has been determined to be 0.05. F_A values have been obtained by measuring the H_2P fluorescence intensity as a function of x in the same sample (containing both QD and H_2P) while performing direct excitation into the H_2P absorption Q band at $\lambda_{ex} = 590$ nm. The experimentally determined H_2P fluorescence intensities have been scaled to the intensities expected for $\lambda_{ex} = 465$ nm while making use of the independently measured ϵ_A of H_2P at both excitation wavelengths at 590 and 465 nm, respectively. The emission intensity at $\lambda_{em} = 651$ nm has been corrected for the residual PL of QD at $\lambda_{em} = 651$ nm as a function of x.

Doing so and assuming $n = 1$, experimentally determined FRET efficiencies E_{FRET} (eq 9) are included in Figure 12 together with the PL quenching efficiency (E) both for YQD

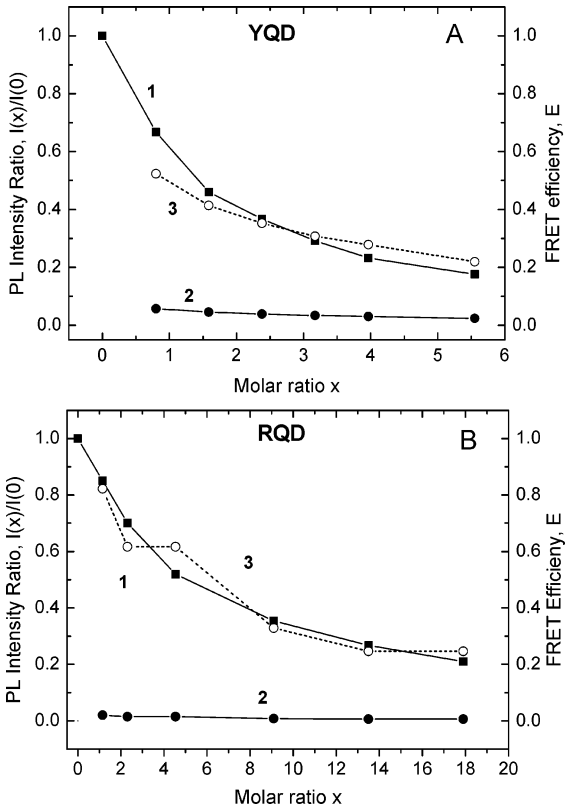

Figure 12. PL intensity ratio $E = I(x)/I(0)$ (1), experimental E_{FRET} (eq 9) (2) and scaled FRET efficiencies (3) for YQD (A) and RQD (B) with $(m\text{-Pyr})_4H_2P$ as a function of the molar ratio (x). Scaling factors are $k = 9.1$ (YQD) and 41.1 (RQD). Details of the procedure are presented in the text.

and RQD. The comparative analysis of these results leads to the following conclusions. In the case of YQD (Figure 12A), E_{FRET} values obtained from H_2P fluorescence enhancement are in the order of 6−8% and thus much smaller as compared to the corresponding QD PL quenching efficiencies ($E = I(x)/I(0)$). For RQD, E_{FRET} values are still much smaller and are estimated to be at 1−2% maximum. With respect to QD PL quenching efficiencies (E), much smaller values of E_{FRET} might be due to three completely different reasons: (i) The presence of two independent quenching processes in the nanoassembly (e.g., FRET and photoinduced charge transfer (CT)). (ii) Some QD show FRET, whereas others are more sensitive to CT. Such an explanation would be in agreement with an inhomogeneous distribution of QD-H_2P nanoassemblies having different local structures and/or environments. (iii) So far we have assumed, neglecting a Poisson distribution, that $n = 1$ corresponds exactly to the molar ratio $x = 1$, which might be not realistic.

To match the E and E_{FRET} efficiencies for YQD (see Figure 12A), the value for n has to be adjusted to n ≈ 0.09, which implies that each QD (on average) contains only 0.09 H_2P molecules. However, it has to be stressed again that this estimation only holds assuming that the QD PL quenching is due only to energy transfer. The value of $n = 0.09$ is in good agreement with $n \approx 0.1$ when adjusting the intrinsic decay component of RQD to the QD PL quenching efficiency (E) observed upon increase of the molar ratio (x) (see previous section 4.2). From this, we conclude that the PL quenching of YQD might be described by FRET. However, in the case of RQD, the corresponding scaling factor to obtain an agreement between the E and E_{FRET} values (see Figure 12B) is much larger and results in $n \approx 0.024$. Whether this procedure is realistic will be discussed later on.

TABLE 2: Number (n) of H_2P Molecules per QD

	YQD	YQD[a]	RQD	RQD[a]
E(cal)[b]	0.2	0.4	0.37	0.74
E_{FRET}(scal)[c]	0.09	0.18	0.024	0.05
time[d]			0.1	0.2

[a] Taking into account a quantum efficiency (φ_D) of 0.5 (see text and Table 1). [b] Calculated $E(x) = I(1)/I_o$ at $x = 1$ while taking k_{DA} from Table 1. [c] Obtained upon scaling of $E_{FRET}(x)$ to $E(x)$ (see text). [d] Fitting the intrinsic PL decay component at $\tau_D^0 \approx 20$ ns to the statistically expected one (see Figure 11).

With respect to FRET, we would like to discuss quantitatively the absolute values of k_{DA} as obtained from a Förster-type approximation. The corresponding data are collected in Table 1. Applying eq 8, we calculate the FRET rates to be $k_{DA} = 5 \times 10^8\ s^{-1}$ for YQD and $0.27 \times 10^8\ s^{-1}$ for RQD. The reduction of k_{DA} for RQD with respect to YQD is due both to the decreased overlap integral ($J(\nu)$) and the increased distance (R_{DA}). These values correspond to $\tau_{DA} \approx 2.0$ and 37 ns for YQD and RQD, respectively. These τ_{DA} times should show up as a decrease of the H_2P fluorescence. In the case of YQD, we were, according to experimental reasons, not able to investigate both time-resolved experiments on YQD and H_2P. The results for RQD have been discussed in the previous chapter. According to the estimation of $\tau_{DA} \approx 37$ ns, we would expect this component to be present in the build up of H_2P fluorescence, which is evidently not seen in Figure 5C. However, this might be due to the fact that in this time regime the remaining RQD PL is superimposed, which decays with $\tau \approx 20-40$ ns.

If we assume that for YQD PL, quenching is merely due to FRET, the experimental quenching efficiency, $E = k_D/(k_D + nk_{DA})$, can be calculated for $k_{DA} = 5 \times 10^8\ s^{-1}$ while assuming $n = 0.2$ at $x = 1$. Applying the same procedure to RQD, it is only possible to approximate the experimental PL quenching efficiency using k_{DA} (RQD) $= 0.27 \times 10^8$ while assuming $n = 0.37$.

Obviously, to explain quenching efficiencies by experimental or calculated FRET efficiencies, one has to decrease (as compared to the molar ratio (x)) the average number (n) of H_2P molecules per QD. Table 2 contains a list of n values as obtained for YQD and RQD. We have also taken into account that because of measured values of QD PL quantum efficiencies ($\varphi_D \approx 0.4-0.5$, see Table 1) the relevant number of H_2P molecules observed in the quenching processes should be $n_{eff} = 2n$ at a given molar ratio. This implies that about half of the H_2P molecules are almost ineffective because they are attached to QD, which is already quenched due to other reasons.

Comparing the results presented in Table 2, we may resume the following. Because calculated Förster rate constants (k_{DA}) are assumed to be correct within at least a factor of 2, the quenching efficiency (E) for YQD can be explained as being due to FRET. For RQD, however, postulated n_{eff} values that simultaneously explain E values (using the calculated FRET rate k_{DA} for $n_{eff} = 0.74$) and the identity of E and E_{FRET} ($n_{eff} = 0.05$) differ from each other by more than a factor of 10. Noteworthy, the analysis of the decay time distribution for RQD results in $n_{eff} \approx 0.2$, which is close to $n_{eff} \approx 0.18$, as obtained for YQD. We therefore assume that $n_{eff} \approx 0.2$ is the most realistic value for both YQD and RQD. This implies, however, that at least for RQD, there are more quenching processes that are effective besides FRET. Interestingly, discrepancies between the FRET results and the quenching efficiencies have also been observed for experiments on QD PL quenching reported recently.[20]

As we have outlined, QD PL quenching is strongly induced by anchoring H_2P molecules depending on both the type of pyridyl substituents and the core/shell diameter of YQD and RQD, respectively. We have also shown that although FRET is a dominant quenching mechanism, at least for YQD, it does not describe the PL quenching efficiency in all cases. An alternative mechanism would be photoinduced charge transfer (CT).[45] Currently, we do not have direct evidence for CT processes. However, some evidence for CT stems from the observed increase of YQD PL quenching when adding acetone, which is more polar than toluene (see Figure 6). It is well known[6,7,41,45] that the solvent polarity increase is often accompanied by an increase in the CT rate. The same argument might apply to the present situation.

Currently, we cannot prove all of the aspects of FRET or CT experimentally in the systems under study. More detailed information will be obtained by systematic measurements on a series of different QD (variation of core and/or shell dimensions) including time-resolved and pump−probe experiments. The most conclusive experiments, however, might be obtained by performing experiments on single nanoassemblies via single molecule/single particle detection. Such experiments have been started but will be extremely complicated.

5. Conclusions

We have shown for the first time in detail that self-assembly principles elaborated for the formation of multichromophoric organic arrays may be extended successfully to organize organic molecules on semiconductor CdSe/ZnS quantum dot surfaces via functionalized anchoring groups in a systematic and directed way. Depending on the CdSe size and the ZnS thickness, the spectral and anchoring properties of dye moieties QD photoluminescence quenching in QD-H_2P nanoassemblies is partly due to fluorescence resonance energy transfer (FRET). However, FRET is also a qualitative tool to identify the well-defined formation of QD-H_2P complexes. A quantitative characterization of FRET and other possible quenching processes will require a systematic variation of QD-dye systems in combination with more elaborated time-resolved experiments. This, however, is beyond the scope of the present publication. Additionally, we would like to point out that single-particle or single-molecule experiments by optical detection of QD and organic dyes, respectively, show that photoinduced CT takes place in the matrix on time scales as long as seconds.[60,61] Whether these processes manifested via "blinking" or luminescence intermittency can be influenced via dye attachments is currently under investigation.

It is also evident from the present experiments that the equilibrium dynamics for the formation of nanoassemblies depend critically on the solvent and the TOPO shell, which will be investigated in forthcoming experiments. One conclusion according to the presented results, however, is that the number of accessible sites on a QD is limited and depends critically on the solvent composition.

Finally, we would like to point out that the tunability of the optical band gap of semiconductor quantum dots via size-dependent quantum confinement (optical tunability), the nearly unlimitted possibilities of physicochemical and structural properties of organic component (chemical tunability) open a stimulating and promising horizon to elaborate organic−inorganic nanoassemblies for possible future practical applications.

Acknowledgment. The experiments have been possible because YQD and RQD were provided by Dr. A. Rogach (Ludwig-Maximilians-University Munich, Germany) and Dr. D. Talapin (Hamburg University, Germany), which is gratefully acknowledged. We also thank Prof. S. Gaponenko (Academy of Sciences, Institute of Molecular and Atomic Physics, Minsk, Belarus) for helpful discussions. D. Starukhin supported the time-resolved experiments. We acknowledge the help of Dr. M. Abdel-Mottaleb, (TU Chemnitz) who provided valuable information on the ligand formation of colloidal QD. Financial support has been provided by the graduate college "Accumulation of single molecules to nanostructures" of the German Science Foundation (T. Blaudeck), the VW-foundation within the research program "Physics, Chemistry and Biology with Single Molecules", the Belarus National Program for Basic and Oriented Research (Nanotech.5.17), and INTAS grant no. 03-50-4540. E.Z. is also thankful to the German Academic Research Service for a DAAD Research Grant (2003).

References and Notes

(1) Brus, L. E.; *Appl. Phys. A*. **1991**, *53*, 465.
(2) Weller, H. *Adv. Mat*. **1993**, *5*, 88.
(3) Hu, J.; Li, L.; Yang, W.; Manna, L.; Alivisatos, A. P. *Science* **2001**, *292*, 2060.
(4) Gaponenko, S. V. *Optical Properties of Semiconductor Nanocrystals*; University Press: Cambridge, England, 1998.
(5) Sessler, J. L.; Wang, B.; Springs, S. L.; Brown, C. T. *Comprehensive Supramolecular Chemistry;* Oxford, England, 1996; p 4311.
(6) Gust, D.; Moore, T. A. In *The Porphyrin Handbook*,. Kadish, K. M., Smith, K. M., Guilard, R., Eds.; Academic Press: New York, 2000; Vol. 8, Chapter 57, pp 153−190.
(7) Zenkevich, E. I.; von Borczyskowski, C. In *Handbook of Polyelectrolytes and Their Applications;* Tripathy, S. K., Kumar, J., Nalwa, H. S., Eds.; American Scientific Publishers: Stevenson Ranch, CA, 2002; Vol. 2, Chapter 11, pp 301−348.
(8) Faure, S.; Stern, C.; Guillard, R.; Harvey, P. D. *J. Am. Chem. Soc*. **2004**, *126*, 1253−1261.
(9) Hayes, R. T.; Walsh, C. J.; Wasielewski, M. R. *J. Phys. Chem. A* **2004**, *108*, 2375−2381.
(10) (a) *An Introduction to Molecular Electronics*; Petty M. C., Bryce M. R., Bloor D., Eds.; Edward Arnold, a division of Holder Headline PLC: London, 1995. (b) Hagfeldt, A., Gratzel, M. *Acc. Chem. Res*. **2000**, *33*, 269−277.
(11) Norris, D. J.; Bawendi, M. G.; Brus, L. E. In *Molecular Electronics*; Jortner, J., Ratner, M., Eds.; Blackwell Science: Cambridge, MA, 2002; p 281.
(12) *Nanoparticles: From Theory to Applications*; Schmid, G., Ed.; Wiley-VCH Verlag: Weinheim, Germany, 2004.
(13) Wojaczynski, J.; Latos-Grazynski, L. *Coord. Chem. Rev*. **2000**, *204*, 113−171.
(14) Chambron, J.-C.; Heitz, V.; Sauvage, J.-P. In *The Porphyrin Handbook*, Kadish, K. M., Smith, K. M., Guilard, R., Eds.; Academic Press: New York, 2000; Vol. 6, Chapter 40, pp 1−40.
(15) Martini, I.; Hodak, J. H.; Hartland, J. V. *J. Phys. Chem. B* **1998**, *102*, 607−614.
(16) Schmeltz, O.; Mews, A.; Basche, T.; Hermann, A.; Mullen, K. *Langmuir* **2001**, *17*, 2861−2865.
(17) Pelet, S.; Moser, J.-E.; Gratzel, M. *J. Phys. Chem. B* **2000**, *104*, 1791.
(18) Javier, A.; Yun, C. S.; Sorena, J.; Strouse, G. F. *J. Phys. Chem. B* **2003**, *107*, 435−442.
(19) Clapp, A. R.; Medintz, I. L.; Mauro, J. M.; Fisher, B. R.; Bawendi, M. G.; Mattoussi, H. *J. Am. Chem. Soc*. **2004**, *126*, 301−310.
(20) Willard, D. M.; Garillo, L. L.; Jung, J.; van Orden, A. *Nano Lett*. **2001**, *1*, 469−474.
(21) Mamedova, N.; Kotov, N. A.; Rogach, A. L.; Studer, J. *Nano Lett*. **2001**, *1*, 281−286.
(22) Sukhanova, A.; Devy, J.; Venteo, L.; Kaplan, H.; Artemyev, M.; Oleinikov, V.; Klimov, D.; Pluot, M.; Cohen, J. H. M.; Nabiev, I. *Anal. Biochem*. **2004**, *324*, 60−67.
(23) (a) Santori, C.; Pelton, M.; Solomon, J.; Dale, Y.; Yamamoto, Y. *Phys. Rev. Lett*. **2001**, *86*, 1502. (b) Larson, D. R.; Zipfel, W. R.; Williams, R. M.; Clark, S. W.; Bruches, M. P.; Wise, F. W.; Webb, W. W. *Science* **2003**, *300*, 1434−1436.
(24) (a) Eisler, H.-J.; Sundar, V. C.; Bawendi, M. G.; Walsh, M.; Smith, H. I.; Klimov, V. *Appl. Phys. Lett*. **2002**, *80*, 4614. (b) Coe-Sullivan, S.; Woo, W.-K.; Steckel, J. S.; Bawendi, M.; Bulovic, V. *Org. Electron*. **2003**, *4*, 123−130.
(25) Rempel, U.; von Maltzan, B.; von Borczyskowski, C. *Pure Appl. Chem*. **1993**, *65*, 1681−1685.

(26) (a) Zenkevich, E. I.; von Borczyskowski, C.; Shulga, A. M.; Bachilo, S. M.; Rempel, U.; Willert, A. *Chem. Phys*. **2002**, *275*, 185−209. (b) Zenkevich, E. I.; von Borczyskowski, C.; Shulga, A. M. *J. Porphyrins Phthalocyanines* **2003**, *7*, 731−754.

(27) Petrov, E.; von Borczyskowski, C.; Zenkevich, E., Shulga, A.; Cichos, F.; Gaponenko, S.; Rogach, A.; Talapin, D.; Weller, H. *Deutsche Physikalische Gesellschaft (DPG)*, Spring Meeting of the Division of Condensed Matter Physics, Dresden, Germany, 2003, CPP 13.4.

(28) Cichos, F.; von Borczyskowski, C.; Petrov, E.; Zenkevich, E.; Shulga, A.; Gaponenko, S.; Rogach, A.; Talapin, D.; Weller, H. *Deutsche Physikalische Gesellschaft (DPG)*, spring meeting of the Division of Condensed Matter Physics, Dresden, Germany, 2003, CPP 22.29.

(29) Talapin, D. V.; Rogach, A. L.; Kornowski, A.; Haase, M.; Weller, H. *Nano Lett*. **2001**, *1*, 207−211.

(30) (a) Gao, M.; Kirstein, S.; Moehwald, H.; Rogach, A. L.; Kornowski, A.; Eychmueller, A.; Weller, H. *J. Phys. Chem. B* **1998**, *102*, 8360. (b) Peng, X.; Manna, L.; Yang, D.; Wickham, J.; Scher, E.; Kadavanich, A.; Alivisatos, A. P. *Nature* **2000**, *404*, 59.

(31) Gao, M.; Lesser, C.; Kirstein, S.; Moehwald, H.; Rogach, A. L.; Weller, H. *J. Appl. Phys*. **2000**, *87*, 2297.

(32) Bowen Katari, J. E.; Colvin, V. L.; Alivisatos, A. P. *J. Phys. Chem.* **1994**, *98*, 4109−4117.

(33) Mikulec, F. V.; Kuno, M.; Bennati, M.; Hall, D. A.; Griffin, R. G.; Bawendi, M. G. *J. Am. Chem. Soc.* **2000**, *122*, 2532.

(34) Yu, W. W.; Qu, L.; Guo, W.; Peng, X. *Chem. Mater*. **2003**, *15*, 2854−2860.

(35) Stirolo, A.; Ward, J.; Prausnitz, J. M.; Parak, W. J.; Zanchet, D.; Gerion, D.; Milliron, D.; Alivisatos, A. P. *J. Phys. Chem. B* **2002**, *106*, 5500−5505.

(36) (a) Little, R. G.; Anton, J. A.; Loach, P. A.; Ibers, J. A. *J. Heterocycl. Chem*. **1975**, *12*, 343−349. (b) Little, R. G. *J. Heterocycl. Chem.* **1981**, *18*, 129−133.

(37) Gardecki, J. A.; Maroncelli, M. *Appl. Spectrosc*. **1998**, *52*, 1700.

(38) Kapitonov, A. M.; Stupak, A. P.; Gaponenko, S. V.; Petrov, E. P.; Rogach, A. L.; Eychmueller, A. *J. Phys. Chem. B* **1999**, *103*, 10109−10113.

(39) Fisher, B. R.; Eisher, H.-J.; Stott, N. E.; Bawendi, M. G. *J. Phys. Chem. B* **2004**, *108*, 143−148.

(40) Gakamski, D. M.; Goldin, A. A.; Petrov, E. P.; Rubinov, A. N. *Biophys. Chem*. **1992**, *44*, 47.

(41) Mattoussi, H.; Cumming, A. W.; Murray, C. B.; Bawendi, M. G.; Ober, R. *Phys. Rev. B* **1998**, *58*, 7850−7863.

(42) Javier, A.; Magana, D.; Jennings, T.; Strouse, J. F. *Appl. Phys. Lett*. **2003**, *83*, 1423−1425.

(43) Petrov, E. P.; Cichos, F.; Rogach, A.; Zenkevich, E.; Starukhin, D.; von Borczyskowski, C. *Chem. Phys. Lett*. **2005**, *402*, 233−238.

(44) Nazzal, A. Y.; Wang, X.; Qu, L.; Yu, W.; Wang, Y.; Peng, X.; Xiao, M. *J. Phys. Chem. B* **2004**, *108*, 5507−5515.

(45) Adams, D.; Brus, L.; Chidsey, C. E. D.; Creager, S.; Greutz, C.; Kagan, C. R.; Kamat, P. V.; Lieberman, M.; Lindsay, S.; Marcus, R. A.; Metzger, R. M.; Michel-Beyerle, M. E.; Miller, J. R.; Newton, M. D.; Rolison, D. R.; Sankey, O.; Schanze, K. S.; Yardley, J.; Zhu, X. *J. Phys. Chem. B* **2003**, *107*, 6668−6697.

(46) Mattoussi, H.; Mauro, J. M.; Goldman, E. R.; Anderson, J. P.; Sundar, V. C.; Mikulec, F. V.; Bawendi, M. G. *J. Am. Chem. Soc*. **2000**, *122*, 12142−12150.

(47) Förster, T. *Modern Quantum Chemistry*; Academic Press: New York, 1965; Vol. 3, p 93.

(48) Lakowicz, J. R. *Principles of Fluorescence Spectroscopy*, 2nd ed.; Kluwer Academic Press: New York, 1999.

(49) Crooker, S. A.; Hollingsworth, J. A.; Tretiak, S.; Klimov, V. I. *Phys. Rev. Lett*. **2002**, *89*, 186802.

(50) Wargnier, R.; Baranov, A. V.; Maslov, V. G.; Stsiapura, V.; Artemyev, M.; Pluot, M.; Sukhanova, A.; Nabiev, I. *Nano Lett*. **2004**, *4*, 451−457.

(51) *The Reaction Center of Photosynthetic Bacteria: Structure and Dynamics*; Michel-Beyerle, M.-E., Ed.; Springer-Verlag: Berlin, Germany, 1996.

(52) Key Ohkubo, K.; Kotani, H.; Shao, J.; Ou, Z.; Kadish, K. M.; Chen, Y.; Zheng, G.; Pandey, R. K.; Fujitsuka, M.; Ito, O.; Imahori, H.; Fukuzumi, S. *Angew. Chem., Int. Ed*. **2004**, *43*, 853−859.

(53) Nirmal, M.; Brus, L. *Acc. Chem. Res*. **1999**, *32*, 407.

(54) Neuhauser, R. G.; Shimizu, K. T.; Woo, W. K.; Empedocles, S. A.; Bawendi, M. G. *Phys. Rev. Lett*. **2000**, *85*, 3301.

(55) Fisher, B. R.; Eisler, H.-J.; Stott, N. E.; Bawendi, M. G. *J. Phys. Chem. B* **2004**, *108*, 143−148.

(56) Cichos, F.; Martin, J.; von Borczyskowski, C. *J. Lumin.* **2004**, *107*, 160−165.

(57) Dexter, D. L. *J. Chem. Phys*. **1953**, *21*, 836.

(58) Sirota, M.; Minkin, E.; Lifshitz, E.; Hensel, V.; Labav, M. *J. Phys. Chem. B* **2001**, *105*, 6792−6797.

(59) Klimov, V. I. *J. Phys. Chem. B* **2000**, *104*, 6112.

(60) Issac, A.; Cichos, F.; von Borczyskowski, C. *Phys. Rev. B.*, **2005**, *71*, in press.

(61) Schuster, J.; Cichos, F.; von Borczyskowski, C. *Opt. Spectrosc.*, in press.